Published in final edited form as:

Hum Genet. 2021 December ; 140(12): 1775–1789. doi:10.1007/s00439-021-02384-y.

WDR37 syndrome: identification of a distinct new cluster of disease-associated variants and functional analyses of mutant proteins

Elena A. Sorokina[1],

Linda M. Reis[1],

Samuel Thompson[1],

Katherine Agre[2],

Dusica Babovic-Vuksanovic[2,3],

Marissa S. Ellingson[3],

Linda Hasadsri[3],

Yolande van Bever[4],

Elena V. Semina[1,5]

[1]Department of Pediatrics and Children's Research Institute, Medical College of Wisconsin, Children's of Wisconsin, Milwaukee, WI, USA

[2]Department of Clinical Genomics, Mayo Clinic, Rochester, MN, USA

[3]Department of Laboratory Medicine and Pathology, Mayo Clinic, Rochester, MN, USA

[4]Department of Clinical Genetics, Erasmus MC University Medical Center, Rotterdam, The Netherlands

[5]Departments of Ophthalmology and Visual Sciences and Cell Biology, Neurobiology and Anatomy, The Medical College of Wisconsin, Milwaukee, WI, USA

Abstract

Missense variants located in the N-terminal region of WDR37 were recently identified to cause a multisystemic syndrome affecting neurological, ocular, gastrointestinal, genitourinary, and cardiac development. *WDR37* encodes a WD40 repeat-containing protein of unknown function.

✉Elena V. Semina, esemina@mcw.edu.

Elena A. Sorokina and Linda M. Reis contributed equally to this work.

Author contributions EVS conceived of and oversaw the work. KA, DBV, YvB provided clinical evaluation and participant referral/enrollment. EAS, LMR, ST performed investigations and analysis of research data; DBV, ME, LH, YvB performed analysis of clinical sequencing data; EVS, EAS, LMR wrote the manuscript with input from all authors.

Conflict of interest The authors have no conflicts of interest to disclose.

Animal research Not applicable.

Ethics approval This study was approved by the Institutional Review Boards of the Children's Hospital of Wisconsin.

Consent to participate Written informed consent was obtained for research analysis.

Consent for publication Consent to publish was obtained from all participants and/or legal guardians; no identifying information is included in this manuscript.

Supplementary Information The online version contains supplementary material available at https://doi.org/10.1007/s00439-021-02384-y.

We identified three novel *WDR37* variants, two likely pathogenic de novo alleles and one inherited variant of uncertain significance, in individuals with phenotypes overlapping those previously reported but clustering in a different region of the protein. The novel alleles are C-terminal to the prior variants and located either within the second WD40 motif (c.659A>G p.(Asp220Gly)) or in a disordered protein region connecting the second and third WD40 motifs (c.778G>A p.(Asp260Asn) and c.770C>A p.(Pro257His)). The three novel mutants showed normal cellular localization but lower expression levels in comparison to wild-type WDR37. To investigate the normal interactions of WDR37, we performed co-immunoprecipitation and yeast two-hybrid assays. This revealed the ability of WDR37 to form homodimers and to strongly bind PACS1 and PACS2 phosphofurin acidic cluster sorting proteins; immunocytochemistry confirmed colocalization of WDR37 with PACS1 and PACS2 in human cells. Next, we analyzed previously reported and novel mutants for their ability to dimerize with wild-type WDR37 and bind PACS proteins. Interaction with wild-type WDR37 was not affected for any variant; however, one novel mutant, p.(Asp220Gly), lost its ability to bind PACS1 and PACS2. In summary, this study presents a novel region of WDR37 involved in human disease, identifies PACS1 and PACS2 as major binding partners of WDR37 and provides insight into the functional effects of various WDR37 variants.

Introduction

WDR37 is a WD40 repeat (WDR) containing protein of unknown function. Missense variants upstream of the first known WD motif (WD1) of *WDR37* were recently identified as a cause of human disease (WDR37 syndrome), characterized by cognitive impairment with early-onset seizures, developmental ocular anomalies including coloboma, corneal opacity, and lens anomalies, structural brain and heart anomalies, feeding issues, dysmorphic facies, and genitourinary defects (Kanca et al. 2019; Reis et al. 2019). Thus far, ten unique individuals have been reported with this rare syndrome in overlapping publications with variants clustered within a span of 16 amino acids from p.Thr115 to p.Thr130 (Aldinger et al. 2019; Hay et al. 2020; Kanca et al. 2019; Reis et al. 2019). Studies in zebrafish confirmed severe effects on development caused by similar missense variants in *wdr37* and identified significant changes in the expression of genes involved in cholesterol biosynthesis in these mutants (Reis et al. 2019); homozygous null mutant *Drosophila* displayed abnormalities in several behavioral phenotypes (bang sensitivity, grip strength, and copulation) which were rescued by wild-type, but not by missense variant cDNA, similarly confirming the deleterious effect of these missense variants (Kanca et al. 2019).

WDR represents one of the most abundant domains within the human proteome (Schapira et al. 2017) and is also present in other eukaryotic kingdoms (Jain and Pandey 2018). WDR domain-containing proteins form a ring structure with four- to eight-bladed β-propellers surrounding a ‘doughnut hole’, which is often the site of interactions with other proteins; a seven-bladed β-propeller structure is most common and predicted to be highly stable structurally (Jain and Pandey 2018). WDR proteins are involved in a wide variety of cellular pathways; the largest numbers of WDR proteins are involved in gene expression, signal transduction, protein metabolism, cell cycle, and immune system pathways, but numerous other pathways also show enrichment for WDR proteins (Schapira et al. 2017). Pathogenic

variants in WDR proteins are linked to diverse human diseases ranging from cancer to developmental disorders affecting the brain and other structures (Al-Rakan et al. 2018; Jain and Pandey 2018; Skraban et al. 2017).

Here, we report two novel de novo likely pathogenic alleles and one inherited variant of uncertain significance located either within the second WDR or in a so-called 'disordered region' connecting the second and third WDRs of WDR37, in a distinct new cluster C-terminal to the prior reported pathogenic alleles; the three variants were identified in individuals affected with severe cognitive impairment and variable syndromic anomalies, expanding both the genetic and phenotypic spectra associated with *WDR37* variants. To further explore the mechanisms of these and previously reported *WDR37* variants, we performed a yeast two-hybrid screen to identify binding factors of WDR37 and utilized this data to test a variety of previously reported and newly identified variants for functional defects.

Materials and methods

Human research

Individuals with variants in *WDR37* (NM_014023.4; build GrCh37) were identified through research analysis at the Medical College of Wisconsin, approved by the Children's Wisconsin Institutional Review Board, or through clinical testing and depositing into Matchmaker Exchange Databases (Philippakis et al. 2015). Written informed consent for research analysis (if applicable) and publication (all) was obtained for every participant. All variants were identified through clinical exome sequencing (Individuals 1 and 2) or research exome sequencing (Individual 3) performed and analyzed as previously described (Reis et al. 2019) and confirmed by Sanger sequencing (Individuals 2 and 3 only). In silico analysis of variants of interest included assessing frequency in the general population in gnomAD v2.1.1 (Karczewski et al. 2020) and predicted effect on protein function by five missense prediction programs (SIFT, Polyphen2, MutationTaster, MutationAssessor, and FATHMM-MKL) and two combined analysis tools for assessing the effect of single nucleotide variants (CADD phred hg19 and REVEL) within dbNSFP (Liu et al. 2013) accessed through the Variant Effect Predictor (McLaren et al. 2016). ACMG/ AMP Guidelines were used in variant interpretation (Richards et al. 2015). *WDR37* genetic variants have been submitted to ClinVar, accession numbers SCV001911449–SCV001911451.

Protein modeling

3D structures for wild-type (NP_054742.2) and mutant (p.(Asp220Gly), p.(Asp260Asn), and p.(Pro257His)) full-length polypeptides were modeled using I-Tasser (Yang et al. 2015) and annotated using Pymol 2.4 (The PyMOL Molecular Graphics System 2021). The location of the WD40 motifs were determined based on UniProt (UniProt 2021).

Yeast 2 hybrid analysis

The yeast two-hybrid screen was performed by Hybrigenics Services SAS (Evry, France). The 1485 base pair (bp) coding sequence (amino acids (aa) 1–494) for the human WDR37 protein (GeneCopoeia, EX-A3878-M14) was subcloned into a pB66 vector as a C-terminal

fusion to the Ga14 DNA-binding domain. This plasmid was used as a bait for screening of the human fetal brain ULTImate library. The bait was neither autoactivating nor toxic, and therefore a tryptophan, leucine, and histidine free selection medium without 3-aminotriazol was used for the screens. The prey fragments were amplified by PCR and sequenced. The GenBank database (NCBI) was used for identification of the DNA fragments. The interacting proteins were assigned a Predicted Biological Score (PBS®), a statistical score reflecting the probability of a significant interaction; the score is grouped into categories according to the degree of confidence in the interaction where PBS® A corresponds to the highest confidence rank, PBS® B to high confidence, PBS® C to good confidence, and PBS® D to low confidence interactions (single interaction) (Formstecher et al. 2005; Rain et al. 2001).

Plasmids and site-directed mutagenesis

pReceiver-M10 cDNA expression vectors containing human WDR37 (GeneCopoeia, EX-A3878-M10), PACS1 (GeneCopoeia, EX-E1384-M10), and PACS2 (GeneCopoeia, EX-I0936-M10) in fusion with Myc-tag were used to express WDR37-Myc, PACS1-Myc, and PACS2-Myc proteins. pReceiver-M14 plasmid containing the full-length WDR37 inserted at HindIII and XbaI sites and fused with 3xFLAG tag (GeneCopoeia, EX-A3878-M14) was used for expression of the FLAG-tagged wild-type WDR37 protein and as a template for site-directed mutagenesis. In vitro site-directed mutagenesis was performed using QuikChange XL Site-Directed Mutagenesis Kit (Agilent Technologies, Santa Clara, CA) and all resulting changes were verified by Sanger sequencing. Mutagenesis primers were designed by the QuikChange Primer Design Program (Agilent Technologies, Santa Clara, CA): for c.659A>G, p.Asp220Gly-5′-agatatgagcagtctgacctccagaagcagtgaga and 5′-tctcactgcttctggaggtcagactgctcatatct, for c.770C>A, p.Pro257His-5′-cccatcgaggtcgtgctcgtccttgtc and 5′-gacaaggacgagcacgacctcgatggg, and for c.778G>A, p.Asp260Asn-5′-gacacatccccattgaggtcgggctcg and 5′-cgagcccgacctcaatggggatgtgtc.

The sequences of the primers used for site-directed mutagenesis of the four N-terminal WDR37 variants (p.Ser119Phe, p.Thr125Ile, p.Ser129Cys, p.Thr130Ile) have been reported previously (Reis et al. 2019).

Cell culture and transfection experiments

B3 human lens epithelial cells (ATCC® CRL-11421™) were grown in Eagle's minimum essential medium (MEM) supplemented with 20% fetal bovine serum. Cells were transfected with plasmid DNA using Lipofectamine 2000 (Thermo Fisher Scientific). For immunoprecipitation experiments, cells at 70–90% confluency growing in a 100 mm cell culture dish were transfected with 6 μg of the plasmid encoding FLAG-tagged protein and 9 μg of the plasmid containing its Myc-tagged binding partner. For immunofluorescence staining, cells growing in 35 mm dishes were transfected with 2.5 μg of each plasmid; after 24 h of incubation and fivefold dilution, cells were transferred into 35 mm Nunc glass-bottom dishes (Thermo Fisher Scientific). Experiments for measuring protein expression levels were done in triplicate by transfecting B3 cells growing in six-well plates with 2.5 μg of each plasmid. The complexes for transfection were prepared by mixing DNA and

Lipofectamine at a 1:2 ratio in Opti-MEM (Invitrogen) according to the manufacturer's recommendations. Cells were harvested 48 h after transfection.

Protein extraction and co-immunoprecipitation

B3 human lens epithelial cells were transiently transfected with plasmids encoding wild-type WDR37-Myc fusion protein and FLAG-tagged WDR37 wild-type or variant proteins. Extracts derived from transfected cells were divided into two equal parts and immunoprecipitated with antibody which recognizes either Myc or FLAG epitopes. Cells were collected by scraping cells from the plate into cold phosphate buffered saline (PBS) solution. The resulting cell suspension was precipitated by centrifugation and the pellet was extracted with 1% Triton X-100 lysis buffer (50 mM HEPES pH 7.4, 150 mM NaCl, 1 mM EGTA, 10% glycerol and 1% Triton X-100) containing protease inhibitor and phosphatase inhibitor cocktails for use with mammalian cell and tissue extracts (Sigma-Aldrich) on ice for 20 min. Lysates were clarified by centrifugation at 12 K, 4 °C and the supernatant was divided into equal parts for overnight immunoprecipitation either with 1 μg of the mouse monoclonal FLAG-M2 antibody (Sigma-Aldrich) or 1 μg monoclonal anti-Myc 9E10 antibody produced in mouse (Santa Cruz Biotechnology). Antibody–protein complexes were captured by incubation with Dynabeads Protein G (Invitrogen by Thermo Fisher Scientific) and washed three times with IP washing buffer [50 mM HEPES pH 7.4, 150 mM NaCl, 1 mM EGTA, 1.5 mM $MgCl_2$, 0.1% Igepal Ca-630 (Sigma-Aldrich)]. Precipitates were released from the beads after incubation in SDS sample buffer at 70 °C for 10 min. For protein expression levels, whole cellular lysates were prepared with RIPA buffer (Thermo Fisher Scientific) in the presence of protease inhibitor cocktail.

The same process was repeated with FLAG-tagged wild-type or variant WDR37 and PACS1-Myc or PACS2-Myc. Cell lysate containing both interacting partners was divided into two parts and precipitated with anti-FLAG or anti-Myc monoclonal antibodies. Control lysates with either WDR37-FLAG or PACS1-Myc expressed alone were precipitated with anti-Myc or anti-FLAG antibodies to rule out any non-specific interactions. Precipitated proteins were subjected to SDS-PAGE and probed with anti-Myc and anti-WDR37 polyclonal antibodies produced in rabbit.

Western blot

Precipitated protein complexes were separated by SDS-PAGE using 18-well 4–15% Criterion Precast Gel (Bio-Rad) followed by an electrophoretic transfer onto an Immobilon-P transfer membrane (Millipore). Blots were blocked in 3% non-fat dry milk and probed either with Myc-Tag (71D10) Rabbit mAb (Cell Signaling) for PACS1-Myc and PACS2-Myc detection or with WDR37 polyclonal antibody produced in rabbit (MyBioSource). Stabilized peroxidase conjugate of the goat anti-rabbit IgG (Thermo Fisher Scientific) was used as a secondary antibody. The signal was detected with iBrightFL1000 imager (Invitrogen) after exposure to the SuperSignal West Femto chemiluminescent substrate ESL reagent (Thermo Fisher Scientific).

To measure the expression of wild-type and mutant WDR37, equal volumes of protein extract were subjected to immunoblot analysis with either anti-Myc or anti-FLAG

antibodies. Western blot on whole cell lysates was done in triplicate and the intensity of the bands was measured by ImageJ software. The FLAG-tagged protein band intensity was normalized by the intensity of the corresponding WDR37-Myc band and these numbers were averaged for each variant. A two-tailed unpaired *t* test was performed using GraphPad Prism version 9.2.0 for Windows, GraphPad Software, San Diego, California USA, www.graphpad.com. For protein molecular weight marker, Precision Plus ProteinTM Standards (Bio-Rad) were utilized.

Immunofluorescence staining

Cells seeded either into glass-bottom dishes as described above or on coverslips were fixed 48 h post-transfection with 4% paraformaldehyde solution in phosphate-buffered saline (PBS) for 10 min. Cells were permeabilized by incubation with 0.25% Triton X-100 for 5 min and non-specific binding sites were blocked with 10% normal goat serum. The intracellular localization of the FLAG-tagged WDR37 mutants was determined by incubation with 20 μg/mL mouse monoclonal FLAG-M2 antibody (Sigma-Aldrich) at 4 °C overnight followed by washes in PBS and incubation with Alexa 568-conjugated donkey anti-mouse IgG (1:1000, Thermo Fisher) at 37 °C for 1 h. In the experiments showing colocalization of Myc-tagged WDR37 and PACS1/PACS2 recombinant proteins, mouse monoclonal anti-Myc 9E10 antibody was used for visualization of WDR37 and either anti-PACS1 or anti-PACS2 rabbit polyclonal antibody (Sigma) for detection of its binding partner. Donkey anti-mouse IgG secondary antibody conjugated with AlexaFluor 568 (Invitrogen) was used for visualization of the targets bound by the mouse antibodies while donkey anti-rabbit IgG secondary antibody conjugated with AlexaFluor 488 (Invitrogen) was used for binding the rabbit antibodies. Cells were covered with DAPI-containing Fluoromount-G (eBioscience) mounting media and imaged with an All-in-One Fluorescence Microscope (Keyence).

Results

Novel variants in WDR37 expand its phenotypic spectrum

We identified two novel de novo variants in *WDR37* and one inherited variant of uncertain significance, all downstream of previously reported variants within the WD2 motif or in the region between WD2 and WD3 (Fig. 1, Table 1).

Individual 1 is a 4-year-old male of Turkish descent with severe developmental delay, microcephaly (45 cm; − 3.72 SD), trigonocephaly, and dysmorphic features. He experienced perinatal asphyxia with hypoglycemia. Brain MRI showed leukoencephalopathy in the parietooccipital, perirolandic, and pre- and post-central gyrus regions and hypoplastic optic nerves; cerebellum, vermis and brainstem were normal as was signal intensity in the neuro and adenohypophysis. He has very poor vision but no other structural ocular anomalies. Height and weight are low-normal (− 2.11 SD and − 2.8 SD, respectively) but limbs are short. At 4 years of age, he could sit and crawl but not walk or pull to stand. He has poor feeding/cannot chew and makes sounds but has no words. He has no history of seizures. Family history was non-contributory. Trio-based exome analysis identified a de novo variant in *WDR37*, Chr10(GRCh37): 1142119A>G, NM_014023.4:c.659A>G p.

(Asp220Gly). Sanger sequencing was not able to be performed but the variant was present in 46 of 81 reads. The variant is not present in gnomAD v2.1.1 and is predicted damaging by 5/5 programs with very high CADD and REVEL scores (32 and 0.946). The variant meets ACMG/AMP criteria to be considered likely pathogenic (PS2, PM2, PP2, PP3). No other pathogenic or likely pathogenic variants were identified to explain the phenotype in this patient.

Individual 2 is a 15-year-old White (US) female born at term with multiple congenital anomalies including Dandy–Walker anomaly, thinning of the corpus callosum, atrial and ventricular septal defects, dysplastic right kidney, tethered cord, cystic ovaries, and bilateral non-obstructing duplicated renal collecting systems. Pregnancy was complicated by hydronephrosis identified at 20 weeks gestation. Apgar scores were 9 and 9. She had hypotonia and significant global developmental delay and is currently non-verbal and non-ambulatory. She has a history of feeding difficulties at 17 months of age, now improved. She is treated for a seizure disorder (onset at 6 years old). She has severe congenital sensorineural hearing loss of the left ear and auditory neuropathy spectrum disorder in the right ear. Dysmorphic features include mild midface hypoplasia, short philtrum, thin lips, downturned corners of the mouth, hypertelorism, overfolded ears, bulbous nose, and dental dysplasia with ocular anomalies consisting of mild bilateral ptosis, bluish sclera, hyperopia, pseudoesotropia, and lower eyelid eversion. The digits are tapered with persistent pads on the fingers, there is mild ulnar deviation of the digits bilaterally, prominent clinodactyly of the fifth digits, and a single transverse crease on both hands. Her height and weight percentiles have varied over time, but have typically been on the low end of normal and she has scoliosis. She is progressing through puberty, but menarche has not occurred. Family history was non-contributory with one unaffected sister. Individual 2 was found to have a heterozygous, de novo *WDR37* variant, Chr10(GRCh37): g.1149593G>A, NM_014023.4: c.778G>A p.(Asp260Asn) detected by reanalysis of trio-based whole exome sequencing and confirmed by Sanger sequencing. The variant was not present in gnomAD v2.1.1 but was only predicted damaging by 2/5 programs (MutationTaster, and Fathmm-MKL) with moderate CADD and REVEL scores (21.8 and 0.193). The variant meets ACMG/AMP criteria to be considered likely pathogenic (PS2, PM2, PP2, PP4). No other pathogenic or likely pathogenic variants were identified to explain the phenotype in this patient.

Individual 3 is a 7-year-old female born at 39 weeks, induced secondary to a known heart defect. She had a complicated neonatal course due to the heart defect and neonatal bacteremia/meningitis (MRSA). She was diagnosed with double outlet right ventricle, tetralogy of Fallot, and pulmonary stenosis and required multiple surgeries to repair. She experienced post-op cardiorespiratory failure requiring ECMO and renal failure/insufficiency following one repair at 8 months of age. At 7 weeks of age, she was diagnosed with a left nuclear dense cataract with synechia between the iris and lens at 10–11 o'clock, removed surgically; the right eye is normal. She failed newborn hearing screening and was diagnosed at 7 weeks of age with profound sensorineural hearing loss ultimately treated with cochlear implant. She also had feeding intolerance with an annular pancreas, dysphagia and duodenal stenosis treated with GJ-tube, recurrent otitis media, scoliosis, and global developmental delay including diagnoses of autism and receptive expressive language disorder. She experienced seizures in the neonatal period and recent

episodes of seizure-like activity. She has limited ambulation with significant hypermobility and has no spoken words. She has a round face, tapering fingers, and fifth finger clinodactyly. Exome sequencing analysis identified a novel inherited variant in *WDR37*, Chr10(GRCh37):g.1149585C>A; NM_014023.4:c.770C>A p.(Pro257His), confirmed by Sanger sequencing in both the child and her unaffected mother with no evidence of mosaicism or reported milder anomalies in the mother. The variant is not present in gnomAD v2.1.1, but is only predicted damaging by 2/5 programs (MutationTaster and fathmm-MKL) with moderate CADD and REVEL scores (20.5 and 0.119, respectively). The variant is considered a variant of uncertain significance under ACMG/AMP guidelines (PM2, PP2, BS2). No other pathogenic or likely pathogenic variants were identified to explain the phenotype in this patient.

***The* in silico *analysis of WDR37 proteins*—**The WDR37 protein contains seven WD40 motifs which encompass amino acids 154–493 and are predicted to fold into a seven-bladed β-propeller structure (Reis et al. 2019); in addition to this, there are two disordered regions spanning amino acids 1–50 and 237–265 (UniProt 2021). The Asp220 affected in Individual 1 is situated within WD40 motif 2 and the other two affected amino acids, Pro257 and Asp260, fall into the disordered region between WD40 motifs 2 and 3 (Fig. 1b, c). All three amino acids are evolutionarily conserved among different species (Fig. 1b), with Asp220 and Asp260 being conserved across vertebrates.

The *in silico* protein modeling predicted significant changes in the tertiary structure of WDR37 as a result of the amino acid substitutions identified in this study (Fig. 2). The p.Asp220Gly substitution (Individual 1) leads to dramatic changes in the whole structure. Blades 1 and 2 of the wild-type propeller and the N-terminus reorganize into a novel six-bladed propeller, while the remaining five blades of the wild-type propeller form a second five-bladed β-propeller. The p.Asp260Asn substitution (Individual 2) causes changes in the position of the N-terminus relative to the propeller structure and results in loss of six of the nine α-helices. Within the WDR domain, blades 3 and 7 each lose a β-sheet, blade 1 loses an α-helix, and blade 6 gains a β-sheet; in addition, amino acids 237–277 form an eighth pseudo-blade within the propeller structure. Finally, the replacement of proline by histidine in position 257 (Individual 3) leads to repositioning of one of the N-terminal α-helixes perpendicular to the inter-blade opening; since this opening is a frequent site of binding in WDR domains (Oliver et al. 2009), this repositioning seems likely to interfere with ligand binding (Fig. 2); the seven-bladed β-propeller is predicted to retain its normal structure in this mutant protein. In summary, *in silico* analysis predicts conformational changes for all variant proteins, particularly the p.Asp220Gly mutant which is expected to form a highly disorganized structure containing two β-propellers (a five- and a six-bladed), erroneously incorporating the N-terminal region into one of them.

Novel WDR37 variant proteins are expressed at a reduced level

To estimate the relative levels of expression, cells were transfected with wild-type WDR37-Myc together with wild-type or variant WDR37-FLAG (Fig. 3A). The expression of wild-type WDR37-Myc was observed at similar levels in all transfections and was used for normalization of wild-type or variant WDR37-FLAG protein expression. All WDR37

FLAG-tagged variant proteins showed a significant reduction in their expression level in comparison to wild-type: to 40% for p.(Asp220Gly) and p.(Pro257His) ($p = 0.0128$ and 0.0019, respectively) and to 30% for p.(Asp260Asn) ($p = 0.0008$) (Fig. 3B).

WDR37 C-terminal variants show normal cellular localization

The subcellular localization of wild-type WDR37 and its novel variants, p.(Asp220Gly), p.(Pro257His) and p.(Asp260Asn), was investigated using transient transfections of the corresponding FLAG-tagged expression plasmids into B3 lens epithelial cells (Fig. 3C). Wild-type and variant recombinant WDR37 were primarily localized in the cytoplasm with the highest concentration in the perinuclear region and in small clusters at the leading edge of the spreading cells (for cells growing either isolated or at the edge of the cell group); weak nuclear presence was also seen. There was no difference in signal distribution observed between wild-type and variant proteins.

WDR37 dimerization is not affected by various disease-associated variants

WDR-containing proteins were previously shown to form dimers (Sejwal et al. 2017; Zhang et al. 2019). Since mutations in the WDR domain could impair dimerization, we tested the binary interactions of wild-type and variant WDR37 (Fig. 4). Co-immunoprecipitation experiments included wild-type and the previously reported N-terminal (p.Ser119Phe, p.Thr125Ile, p.Ser129Cys, p.Thr130Ile) as well as the newly identified C-terminal (p.Asp220Gly p.Pro257His and p.Asp260Asn) variants. Immunoprecipitation with anti-Myc antibodies captured FLAG-tagged wild-type WDR37 as well as all variant proteins (Fig. 4A). In control immunoprecipitation, when FLAG-tagged wild-type WDR37 was expressed alone, no precipitation by antibodies against the Myc-epitope was observed, showing specificity of the binding. This result demonstrates that dimerization with wild-type WDR37 is not affected by any of the studied N- or C-terminal missense variants.

Identification of WDR37 interacting partners via yeast two-hybrid screen

In a yeast two-hybrid screen, full-length human WDR37 was used as a bait against a human fetal brain cDNA library. 72 positive clones were detected from among 113 million tested interactions (Supplementary Table 1). Out of these, 60 clones were identified as PACS1 with Predicted Biological Score (PBS®) A and another seven clones as PACS2 with PBS® B. Other interactions included two clones identified as collagen type XII alpha 1 chain, COL12A1, with PBS® C and two other proteins, eukaryotic translation initiation factor 4 gamma 3 (EIF4G3) and thyroid hormone receptor interactor 11 (TRIP11), both represented by a single clone and hence assigned PBS® category D (Supplementary Table 1). PACS1 and PACS2, phosphofurin acidic cluster sorting proteins 1 and 2, correspondingly, are involved in the sorting of proteins which contain acidic cluster sorting (ACS) motifs. Since both PACS1 and PACS2 showed the strongest confidence interactions with WDR37, we focused on these proteins in our further studies.

WDR37 colocalizes with PACS1 and PACS2

The relative intracellular distribution of WDR37 and PACS1 or PACS2 was investigated using human lens epithelial cells. Myc-tagged wild-type WDR37 was expressed in B3 lens

epithelial cells and immunofluorescent staining was performed to visualize endogenous PACS1 or PACS2 and WDR37-Myc (Fig. 4B). All proteins were localized predominantly in the cytoplasm around the nucleus (with some weak nuclear presence) with a small amount of WDR37, PACS1 and PACS2 also found at the leading edge of the spreading cells; superposition of fluorescence images confirmed colocalization in these compartments (Fig. 4B). This is consistent with prior studies that detected PACS1 primarily in the perinuclear region extending into the cell periphery (Crump et al. 2001; Wan et al. 1998), but also able to shuttle between the nucleus and cytoplasm (Liu et al. 2020), consistent with the weak nuclear stain. Similarly, while PACS2 was able to translocate to the nucleus in response to the stress condition, it was originally described as an endoplasmic reticulum (ER) and cytosolic protein which controls the apposition of mitochondria with the ER (Atkins et al. 2014; Simmen et al. 2005).

Together, these results support the predicted interaction of WDR37 with both PACS1 and PACS2 by demonstrating significant colocalization of these proteins within the cell.

Examination of WDR37 wild-type and mutant interactions with PACS1 and PACS2

Co-immunoprecipitation experiments were performed to validate the yeast two-hybrid results for wild-type WDR37 and PACS1 and PACS2 proteins, as well as to test if/how these interactions are affected by WDR37 disease-associated variants (Fig. 4C, D). FLAG-tagged wild-type or variant WDR37 (p.Ser119Phe, p.Thr125Ile, p.Ser129Cys, p.Thr130Ile, p.Asp220Gly, p.Pro257His, and p.Asp260Asn) and PACS1-Myc or PACS2-Myc were pairwise expressed in B3 lens epithelial cells. Both interacting partners were co-immunoprecipitated with anti-FLAG and anti-Myc antibodies. Neither WDR37-FLAG nor PACS1-Myc or PACS2-Myc were precipitated with antibody directed against its binding partner when expressed alone. Western blot analysis confirmed successful precipitation of the targeted antigens. FLAG-tagged p.Ser119Phe, p.Thr125Ile, p.Ser129Cys, p.Thr130Ile, p.Pro257His and p.Asp260Asn WDR37 variants were co-precipitated with both PACS1-Myc and PACS2-Myc with the same efficiency as wild-type WDR37-FLAG. However, p.Asp220Gly failed to co-precipitate with either PACS1 or PACS2. This indicates that either residue Asp220 in WDR37 has a critical role in its interaction with both PACS1 and PACS2 or that the conformational changes caused by this substitution preclude its binding with these partners.

Discussion

While the variants identified in this study affect a new region of the WDR37 protein, there is considerable phenotypic overlap with the ten previously reported cases with WDR37 syndrome (Hay et al. 2020; Kanca et al. 2019; Reis et al. 2019). Similar to previous cases, all three individuals have severe developmental delay/cognitive impairment with limited to no ambulation and all are non-verbal. Interestingly, Individual 1, with the only variant shown to disrupt interaction with PACS1 and PACS2 and the strongest *in silico* predictions to date, seems to have the least syndromic phenotype and is the only individual without seizures; however, his microcephaly, optic nerve hypoplasia, mildly short stature, and feeding disorder are consistent with WDR37 syndrome. While the variants in Individuals 2 and 3 have

weaker functional predictions, they show stronger phenotypic overlap with the previously reported cases including seizures, hearing loss, scoliosis, heart defects, tapered fingers, and feeding disorder along with variable kidney, ocular, and gastrointestinal structural anomalies. One previously reported variant, c.344C>T p.(Thr115Ile), had similarly weak *in silico* predictions (damaging by 3/5, CADD score 23.2, REVEL score 0.263) and no previously reported variant had a REVEL score higher than 0.503 (range 0.263–0.503, mean 0.4239, median 0.4545; Table 1), suggesting that *in silico* analysis may be less accurate for this gene and may not adequately capture the mechanism of pathogenicity. Overall, the ocular anomalies are milder in this cohort (no coloboma or microphthalmia) and the structural brain anomalies in Individuals 1 and 3 also seem to be milder than those previously reported (Hay et al. 2020).

The de novo variants identified in individuals 1 and 2 meet ACMG/AMP criteria to be considered likely pathogenic, but the significance of the inherited variant identified in Individual 3 is uncertain. Although *in silico* modeling, functional data, and phenotypic overlap do suggest a role for *WDR37* in the phenotype, since the variant was inherited from an unaffected parent, the significance is unclear. It is possible that incomplete penetrance, mosaicism, or a second hit (either genetic or environmental) could play a role in the differing phenotypes between the child and her mother. For example, the clinical phenotype may be a result of the combination of the neonatal meningitis and this genetic variant; it is also possible that this *WDR37* allele is a rare benign variant unrelated to the patient's phenotype.

Although a dominant negative effect for the previously reported missense alleles has been suggested (Kanca et al. 2019; Reis et al. 2019), the mechanism of action has not been established for either the previously reported or the novel variants reported here. This study identified slightly decreased expression but normal localization for the novel mutants; the N-terminal mutants were previously shown to have comparable expression and localization to wild-type (Reis et al. 2019). Since other WDR domain proteins form dimers through either the C-terminal WDR domain or the N-terminal coiled-coil domain (Parkhouse et al. 2013), we tested the ability of WDR37 mutant proteins to form dimers with wild-type WDR37 and determined that dimerization with wild-type WDR37 was not affected by any of the missense variants studied, supporting the possibility of a dominant negative effect.

To further investigate the mechanism of disease, we undertook a yeast two-hybrid screen to reveal binding partners of wild-type WDR37. This experiment identified phosphofurin acidic cluster sorting proteins 1 and 2 (PACS1 and PACS2) as the only major binding factors of WDR37 in the fetal brain. WDR37 was previously found to interact with both PACS1 and PACS2 through a high-throughput affinity-purification mass spectrometry study (Huttlin et al. 2015) and, more recently, Wdr37 and Pacs1 interaction was demonstrated through forward genetic screening in mice (Nair-Gill et al. 2021).

PACS1 and PACS2 are both involved in the sorting of proteins which contain acidic cluster sorting (ACS) motifs (Crump et al. 2001; Kottgen et al. 2005; Piguet et al. 2000). PACS1 is a multifunctional connector protein which is involved in the cytosolic transport and ciliary trafficking of proteins containing ACS motifs (Crump et al. 2001; Jenkins et al. 2009;

Schermer et al. 2005; Wan et al. 1998). PACS2 similarly controls protein trafficking from the endoplasmic reticulum (ER) to mitochondria by acting as a tether (Simmen et al. 2005). In addition to their primary roles in the cytoplasm, PACS1 and PACS2 can also accumulate in the nucleus in response to DNA damage and PACS1 was shown to participate in the nuclear export of HIV-1 transcripts (Atkins et al. 2014; Liu et al. 2020; Mani et al. 2020). Both proteins share a high degree of homology with 54% sequence identity and both possess a 140 amino acid cargo-binding region which is necessary for acidic cluster sorting motif recognition.

Disruption of *PACS1* and *PACS2* also result in human diseases: autosomal dominant Schuurs-Hoeijmakers syndrome and autosomal dominant Developmental and Epileptic Encephalopathy 66, respectively (Olson et al. 2018; Schuurs-Hoeijmakers et al. 2016). Both conditions are caused by recurrent de novo missense variants and both show remarkable overlap with the clinical features caused by pathogenic variants in the *WDR37* gene. All three disorders result in cognitive impairment, structural brain anomalies, and overlapping dysmorphic facial features including arching eyebrows, hypertelorism, a broad nasal root, a thin upper lip, and downturned mouth; while ocular coloboma, heart defects, poor growth, and genitourinary anomalies are noted in all three conditions, they are much more penetrant in *WDR37* syndrome and seizures are seen only in *WDR37* and *PACS2*-related disorders (Sakaguchi et al. 2021). Current evidence suggests a dominant negative mechanism for known PACS1/2 diseases: for both genes, a specific missense variant is identified as the cause of all but one case (with a closely related variant), expression of dominant negative PACS1 was shown to result in mislocalization of integral membrane proteins such as furin and mannose-6-phosphate receptor within the cell (Crump et al. 2001), and a recent study found that a multi-exon deletion predicted to result in loss of function of *PACS1* did not result in features of Schuurs–Hoeijmakers syndrome in a three-generation family (Liu et al. 2021). The strong degree of phenotypic overlap as well as consistent evidence of interaction between WDR37 and PACS1/2 suggests that WDR37 may also be involved in protein transport and that the identified missense variants in these proteins disrupt their function through a dominant negative mechanism.

Our data identifies a novel disease-associated region of *WDR37*, C-terminal to the previously reported cluster, with two de novo likely pathogenic variants and one variant of uncertain significance, and supports previous studies by identifying PACS1 and PACS2 as the major interacting partners of WDR37. One of the novel variants, p.Asp220Gly, disrupted interaction of WDR37 with both PACS1 and PACS2 proteins. However, the significance of this finding is currently unclear since all other mutants showed normal binding capabilities with these proteins. Further work is needed to determine the role of PACS binding in the normal function of WDR37 and the mechanism of action for various pathogenic variants in *WDR37*.

Supplementary Material

Refer to Web version on PubMed Central for supplementary material.

Acknowledgements

We are grateful to the patients and their families for participation in this study. This work was supported by National Institutes of Health grants R21HD099701 and R01EY025718 as well as funds provided by the Children's Research Institute Foundation at Children's Wisconsin (EVS) and 1UL1RR031973 from the Clinical and Translational Science Award (CTSA) program.

Funding

This work was supported by NIH grants R21HD099701 and R01EY025718 as well as funds provided by the Children's Research Institute Foundation at Children's Wisconsin (EVS) and NIH grant 1UL1RR031973 from the Clinical and Translational Science Award (CTSA) program.

Availability of data and material

There are no other data associated with this manuscript. *WDR37* genetic variants have been submitted to ClinVar, accession numbers SCV001911449–SCV001911451.

References

Aldinger KA, Timms AE, Thomson Z, Mirzaa GM, Bennett JT, Rosenberg AB, Roco CM, Hirano M, Abidi F, Haldipur P, Cheng CV, Collins S, Park K, Zeiger J, Overmann LM, Alkuraya FS, Biesecker LG, Braddock SR, Cathey S, Cho MT, Chung BHY, Everman DB, Zarate YA, Jones JR, Schwartz CE, Goldstein A, Hopkin RJ, Krantz ID, Ladda RL, Leppig KA, McGillivray BC, Sell S, Wusik K, Gleeson JG, Nickerson DA, Bamshad MJ, Gerrelli D, Lisgo SN, Seelig G, Ishak GE, Barkovich AJ, Curry CJ, Glass IA, Millen KJ, Doherty D, Dobyns WB (2019) Redefining the etiologic landscape of cerebellar malformations. Am J Hum Genet 105:606–615. 10.1016/j.ajhg.2019.07.019 [PubMed: 31474318]

Al-Rakan MA, Abothnain MD, Alrifai MT, Alfadhel M (2018) Extending the ophthalmological phenotype of Galloway-Mowat syndrome with distinct retinal dysfunction: a report and review of ocular findings. BMC Ophthalmol 18:147. 10.1186/s12886-018-0820-4 [PubMed: 29929488]

Atkins KM, Thomas LL, Barroso-Gonzalez J, Thomas L, Auclair S, Yin J, Kang H, Chung JH, Dikeakos JD, Thomas G (2014) The multifunctional sorting protein PACS-2 regulates SIRT1-mediated deacetylation of p53 to modulate p21-dependent cell-cycle arrest. Cell Rep 8:1545–1557. 10.1016/j.celrep.2014.07.049 [PubMed: 25159152]

Crump CM, Xiang Y, Thomas L, Gu F, Austin C, Tooze SA, Thomas G (2001) PACS-1 binding to adaptors is required for acidic cluster motif-mediated protein traffic. EMBO J 20:2191–2201. 10.1093/emboj/20.9.2191 [PubMed: 11331585]

Formstecher E, Aresta S, Collura V, Hamburger A, Meil A, Trehin A, Reverdy C, Betin V, Maire S, Brun C, Jacq B, Arpin M, Bellaiche Y, Bellusci S, Benaroch P, Bornens M, Chanet R, Chavrier P, Delattre O, Doye V, Fehon R, Faye G, Galli T, Girault JA, Goud B, de Gunzburg J, Johannes L, Junier MP, Mirouse V, Mukherjee A, Papadopoulo D, Perez F, Plessis A, Rosse C, Saule S, Stoppa-Lyonnet D, Vincent A, White M, Legrain P, Wojcik J, Camonis J, Daviet L (2005) Protein interaction mapping: a Drosophila case study. Genome Res 15:376–384. 10.1101/gr.2659105 [PubMed: 15710747]

Hay E, Henderson RH, Mansour S, Deshpande C, Jones R, Nutan S, Mankad K, Young RM, Moosajee M, Research Consortium GE, Arno G (2020) Expanding the phenotypic spectrum consequent upon de novo WDR37 missense variants. Clin Genet 98:191–197. 10.1111/cge.13795 [PubMed: 32530092]

Huttlin EL, Ting L, Bruckner RJ, Gebreab F, Gygi MP, Szpyt J, Tam S, Zarraga G, Colby G, Baltier K, Dong R, Guarani V, Vaites LP, Ordureau A, Rad R, Erickson BK, Wuhr M, Chick J, Zhai B, Kolippakkam D, Mintseris J, Obar RA, Harris T, Artavanis-Tsakonas S, Sowa ME, De Camilli P, Paulo JA, Harper JW, Gygi SP (2015) The BioPlex network: a systematic exploration of the human interactome. Cell 162:425–440. 10.1016/j.cell.2015.06.043 [PubMed: 26186194]

Jain BP, Pandey S (2018) WD40 repeat proteins: signalling scaffold with diverse functions. Protein J 37:391–406. 10.1007/s10930-018-9785-7 [PubMed: 30069656]

Jenkins PM, Zhang L, Thomas G, Martens JR (2009) PACS-1 mediates phosphorylation-dependent ciliary trafficking of the cyclic-nucleotide-gated channel in olfactory sensory neurons. J Neurosci 29:10541–10551. 10.1523/JNEUROSCI.1590-09.2009 [PubMed: 19710307]

Kanca O, Andrews JC, Lee PT, Patel C, Braddock SR, Slavotinek AM, Cohen JS, Gubbels CS, Aldinger KA, Williams J, Indaram M, Fatemi A, Yu TW, Agrawal PB, Vezina G, Simons C, Crawford J, Lau CC, Undiagnosed Diseases N, Chung WK, Markello TC, Dobyns WB, Adams DR, Gahl WA, Wangler MF, Yamamoto S, Bellen HJ, Malicdan MCV (2019) De Novo Variants in WDR37 Are Associated with Epilepsy, Colobomas, Dysmorphism, developmental delay, intellectual disability, and cerebellar hypoplasia. Am J Hum Genet 105:413–424. 10.1016/j.ajhg.2019.06.014 [PubMed: 31327508]

Karczewski KJ, Francioli LC, Tiao G, Cummings BB, Alfoldi J, Wang Q, Collins RL, Laricchia KM, Ganna A, Birnbaum DP, Gauthier LD, Brand H, Solomonson M, Watts NA, Rhodes D, Singer-Berk M, England EM, Seaby EG, Kosmicki JA, Walters RK, Tashman K, Farjoun Y, Banks E, Poterba T, Wang A, Seed C, Whiffin N, Chong JX, Samocha KE, Pierce-Hoffman E, Zappala Z, O'Donnell-Luria AH, Minikel EV, Weisburd B, Lek M, Ware JS, Vittal C, Armean IM, Bergelson L, Cibulskis K, Connolly KM, Covarrubias M, Donnelly S, Ferriera S, Gabriel S, Gentry J, Gupta N, Jeandet T, Kaplan D, Llanwarne C, Munshi R, Novod S, Petrillo N, Roazen D, Ruano-Rubio V, Saltzman A, Schleicher M, Soto J, Tibbetts K, Tolonen C, Wade G, Talkowski ME, Genome Aggregation Database C, Neale BM, Daly MJ, MacArthur DG (2020) The mutational constraint spectrum quantified from variation in 141,456 humans. Nature 581:434–443. 10.1038/s41586-020-2308-7 [PubMed: 32461654]

Kottgen M, Benzing T, Simmen T, Tauber R, Buchholz B, Feliciangeli S, Huber TB, Schermer B, Kramer-Zucker A, Hopker K, Simmen KC, Tschucke CC, Sandford R, Kim E, Thomas G, Walz G (2005) Trafficking of TRPP2 by PACS proteins represents a novel mechanism of ion channel regulation. EMBO J 24:705–716. 10.1038/sj.emboj.7600566 [PubMed: 15692563]

Liu X, Jian X, Boerwinkle E (2013) dbNSFP v2.0: a database of human non-synonymous SNVs and their functional predictions and annotations. Hum Mutat 34:E2393–E2402. 10.1002/humu.22376;10.1002/humu.22376 [PubMed: 23843252]

Liu H, Hu PW, Budhiraja S, Misra A, Couturier J, Lloyd RE, Lewis DE, Kimata JT, Rice AP (2020) PACS1 is an HIV-1 cofactor that functions in Rev-mediated nuclear export of viral RNA. Virology 540:88–96. 10.1016/j.virol.2019.10.004 [PubMed: 31759187]

Liu Y, Ding H, Yan T, Liu L, Yu L, Huang Y, Li F, Zeng Y, Huang W, Zhang Y, Yin A (2021) A Novel Multi-Exon Deletion of PACS1 in a three-generation pedigree: supplements to PACS1 neurodevelopmental disorder spectrum. Front Genet 12:690216. 10.3389/fgene.2021.690216 [PubMed: 34373684]

Mani C, Tripathi K, Luan S, Clark DW, Andrews JF, Vindigni A, Thomas G, Palle K (2020) The multifunctional protein PACS-1 is required for HDAC2- and HDAC3-dependent chromatin maturation and genomic stability. Oncogene 39:2583–2596. 10.1038/s41388-020-1167-x [PubMed: 31988453]

McLaren W, Gil L, Hunt SE, Riat HS, Ritchie GR, Thormann A, Flicek P, Cunningham F (2016) The Ensembl Variant Effect Predictor. Genome Biol 17:122. 10.1186/s13059-016-0974-4 [PubMed: 27268795]

Nair-Gill E, Bonora M, Zhong X, Liu A, Miranda A, Stewart N, Ludwig S, Russell J, Gallagher T, Pinton P, Beutler B (2021) Calcium flux control by Pacs1-Wdr37 promotes lymphocyte quiescence and lymphoproliferative diseases. EMBO J 40:e104888. 10.15252/embj.2020104888 [PubMed: 33630350]

Oliver AW, Swift S, Lord CJ, Ashworth A, Pearl LH (2009) Structural basis for recruitment of BRCA2 by PALB2. EMBO Rep 10:990–996. 10.1038/embor.2009.126 [PubMed: 19609323]

Olson HE, Jean-Marcais N, Yang E, Heron D, Tatton-Brown K, van der Zwaag PA, Bijlsma EK, Krock BL, Backer E, Kamsteeg EJ, Sinnema M, Reijnders MRF, Bearden D, Begtrup A, Telegrafi A, Lunsing RJ, Burglen L, Lesca G, Cho MT, Smith LA, Sheidley BR, Moufawad El Achkar C, Pearl PL, Poduri A, Skraban CM, Tarpinian J, Nesbitt AI, Fransen van de Putte DE, Ruivenkamp CAL, Rump P, Chatron N, Sabatier I, De Bellescize J, Guibaud L, Sweetser DA, Waxler JL, Wierenga KJ, Study DDD, Donadieu J, Narayanan V, Ramsey KM, Group CRR, Nava C, Riviere JB, Vitobello A, Tran Mau-Them F, Philippe C, Bruel AL, Duffourd Y, Thomas L, Lelieveld SH,

Schuurs-Hoeijmakers J, Brunner HG, Keren B, Thevenon J, Faivre L, Thomas G, Thauvin-Robinet C (2018) A recurrent de novo PACS2 heterozygous missense variant causes neonatal-onset developmental epileptic encephalopathy, facial dysmorphism, and cerebellar dysgenesis. Am J Hum Genet 102: 995–1007. 10.1016/j.ajhg.2018.03.005 [PubMed: 29656858]

Parkhouse R, Ebong IO, Robinson CV, Monie TP (2013) The N-terminal region of the human autophagy protein ATG16L1 contains a domain that folds into a helical structure consistent with formation of a coiled-coil. PLoS ONE 8:e76237. 10.1371/journal.pone.0076237 [PubMed: 24086718]

Philippakis AA, Azzariti DR, Beltran S, Brookes AJ, Brownstein CA, Brudno M, Brunner HG, Buske OJ, Carey K, Doll C, Dumitriu S, Dyke SO, den Dunnen JT, Firth HV, Gibbs RA, Girdea M, Gonzalez M, Haendel MA, Hamosh A, Holm IA, Huang L, Hurles ME, Hutton B, Krier JB, Misyura A, Mungall CJ, Paschall J, Paten B, Robinson PN, Schiettecatte F, Sobreira NL, Swaminathan GJ, Taschner PE, Terry SF, Washington NL, Zuchner S, Boycott KM, Rehm HL (2015) The Matchmaker exchange: a platform for rare disease gene discovery. Hum Mutat 36:915–921. 10.1002/humu.22858 [PubMed: 26295439]

Piguet V, Wan L, Borel C, Mangasarian A, Demaurex N, Thomas G, Trono D (2000) HIV-1 Nef protein binds to the cellular protein PACS-1 to downregulate class I major histocompatibility complexes. Nat Cell Biol 2:163–167. 10.1038/35004038 [PubMed: 10707087]

Rain JC, Selig L, De Reuse H, Battaglia V, Reverdy C, Simon S, Lenzen G, Petel F, Wojcik J, Schachter V, Chemama Y, Labigne A, Legrain P (2001) The protein-protein interaction map of Helicobacter pylori. Nature 409:211–215. 10.1038/35051615 [PubMed: 11196647]

Reis LM, Sorokina EA, Thompson S, Muheisen S, Velinov M, Zamora C, Aylsworth AS, Semina EV (2019) De Novo Missense Variants in WDR37 cause a severe multisystemic syndrome. Am J Hum Genet 105:425–433. 10.1016/j.ajhg.2019.06.015 [PubMed: 31327510]

Richards S, Aziz N, Bale S, Bick D, Das S, Gastier-Foster J, Grody WW, Hegde M, Lyon E, Spector E, Voelkerding K, Rehm HL (2015) Standards and guidelines for the interpretation of sequence variants: a joint consensus recommendation of the American College of Medical Genetics and Genomics and the Association for Molecular Pathology. Genet Med 17:405–424. 10.1038/gim.2015.30 [PubMed: 25741868]

Sakaguchi Y, Yoshihashi H, Uehara T, Miyama S, Kosaki K, Takenouchi T (2021) Coloboma may be a shared feature in a spectrum of disorders caused by mutations in the WDR37-PACS1-PACS2 axis. Am J Med Genet A 185:884–888. 10.1002/ajmg.a.62020 [PubMed: 33369122]

Schapira M, Tyers M, Torrent M, Arrowsmith CH (2017) WD40 repeat domain proteins: a novel target class? Nat Rev Drug Discov 16:773–786. 10.1038/nrd.2017.179 [PubMed: 29026209]

Schermer B, Hopker K, Omran H, Ghenoiu C, Fliegauf M, Fekete A, Horvath J, Kottgen M, Hackl M, Zschiedrich S, Huber TB, Kramer-Zucker A, Zentgraf H, Blaukat A, Walz G, Benzing T (2005) Phosphorylation by casein kinase 2 induces PACS-1 binding of nephrocystin and targeting to cilia. EMBO J 24:4415–4424. 10.1038/sj.emboj.7600885 [PubMed: 16308564]

Schuurs-Hoeijmakers JH, Landsverk ML, Foulds N, Kukolich MK, Gavrilova RH, Greville-Heygate S, Hanson-Kahn A, Bernstein JA, Glass J, Chitayat D, Burrow TA, Husami A, Collins K, Wusik K, van der Aa N, Kooy F, Brown KT, Gadzicki D, Kini U, Alvarez S, Fernandez-Jaen A, McGehee F, Selby K, Tarailo-Graovac M, Van Allen M, van Karnebeek CD, Stavropoulos DJ, Marshall CR, Merico D, Gregor A, Zweier C, Hopkin RJ, Chu YW, Chung BH, de Vries BB, Devriendt K, Hurles ME, Brunner HG, study DDD (2016) Clinical delineation of the PACS1-related syndrome—report on 19 patients. Am J Med Genet A 170:670–675. 10.1002/ajmg.a.37476 [PubMed: 26842493]

Sejwal K, Chami M, Remigy H, Vancraenenbroeck R, Sibran W, Sutterlin R, Baumgartner P, McLeod R, Chartier-Harlin MC, Baekelandt V, Stahlberg H, Taymans JM (2017) Cryo-EM analysis of homodimeric full-length LRRK2 and LRRK1 protein complexes. Sci Rep 7:8667. 10.1038/s41598-017-09126-z [PubMed: 28819229]

Simmen T, Aslan JE, Blagoveshchenskaya AD, Thomas L, Wan L, Xiang Y, Feliciangeli SF, Hung CH, Crump CM, Thomas G (2005) PACS-2 controls endoplasmic reticulum-mitochondria communication and Bid-mediated apoptosis. EMBO J 24:717–729. 10.1038/sj.emboj.7600559 [PubMed: 15692567]

Skraban CM, Wells CF, Markose P, Cho MT, Nesbitt AI, Au PYB, Begtrup A, Bernat JA, Bird LM, Cao K, de Brouwer APM, Denenberg EH, Douglas G, Gibson KM, Grand K, Goldenberg A, Innes AM, Juusola J, Kempers M, Kinning E, Markie DM, Owens MM, Payne K, Person R, Pfundt R, Stocco A, Turner CLS, Verbeek NE, Walsh LE, Warner TC, Wheeler PG, Wieczorek D, Wilkens AB, Zonneveld-Huijssoon E, Deciphering Developmental Disorders S, Kleefstra T, Robertson SP, Santani A, van Gassen KLI, Deardorff MA (2017) WDR26 Haploinsufficiency causes a recognizable syndrome of intellectual disability, seizures, abnormal gait, and distinctive facial features. Am J Hum Genet 101:139–148. 10.1016/j.ajhg.2017.06.002 [PubMed: 28686853]

The PyMOL Molecular Graphics System VS, LLC (2021) The PyMOL Molecular Graphics System, Version 2.0. Schrödinger, LLC

UniProt C (2021) UniProt: the universal protein knowledgebase in 2021. Nucleic Acids Res 49:D480–D489. 10.1093/nar/gkaa1100 [PubMed: 33237286]

Wan L, Molloy SS, Thomas L, Liu G, Xiang Y, Rybak SL, Thomas G (1998) PACS-1 defines a novel gene family of cytosolic sorting proteins required for trans-Golgi network localization. Cell 94:205–216. 10.1016/s0092-8674(00)81420-8 [PubMed: 9695949]

Yang J, Yan R, Roy A, Xu D, Poisson J, Zhang Y (2015) The I-TASSER Suite: protein structure and function prediction. Nat Methods 12:7–8. 10.1038/nmeth.3213 [PubMed: 25549265]

Zhang P, Fan Y, Ru H, Wang L, Magupalli VG, Taylor SS, Alessi DR, Wu H (2019) Crystal structure of the WD40 domain dimer of LRRK2. Proc Natl Acad Sci USA 116:1579–1584. 10.1073/pnas.1817889116 [PubMed: 30635421]

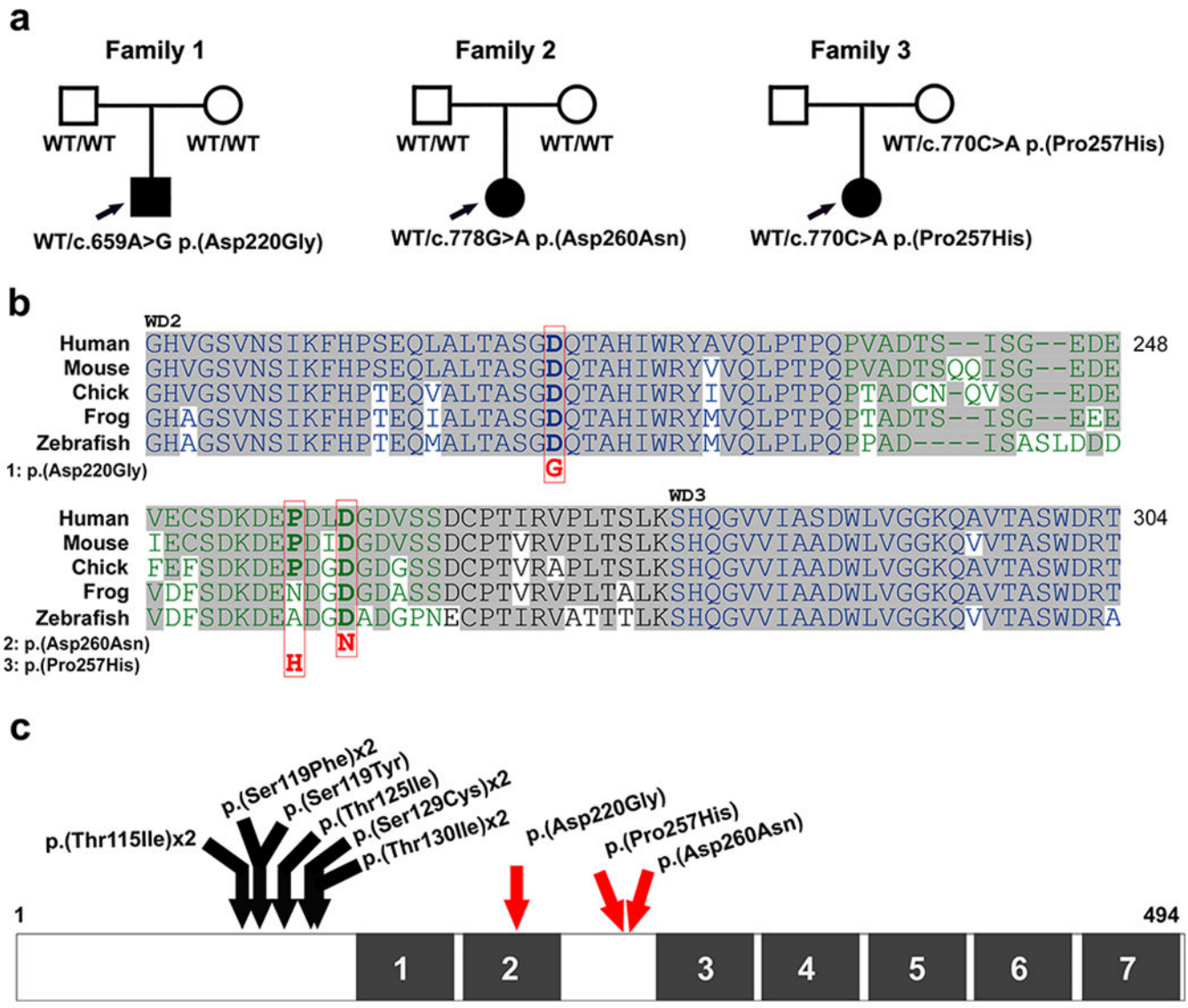

Fig. 1.

Identification of novel *WDR37* variants. **a** Human pedigrees (Individuals 1–3 are marked with arrows in respective pedigrees (Families 1–3)); filled symbol indicates affected individuals, WT indicates wild-type allele. **b** Multispecies alignment showing conservation of affected amino acids; WD40 motifs are shown in blue text, ‘disordered region’ between WD2 and WD3 in green text, and conserved amino acids with gray shading. **c** Schematic drawing of WDR37 protein with new (red arrows) and previously identified (black arrows) alleles indicated; black boxes indicate seven consecutive WD40 motifs

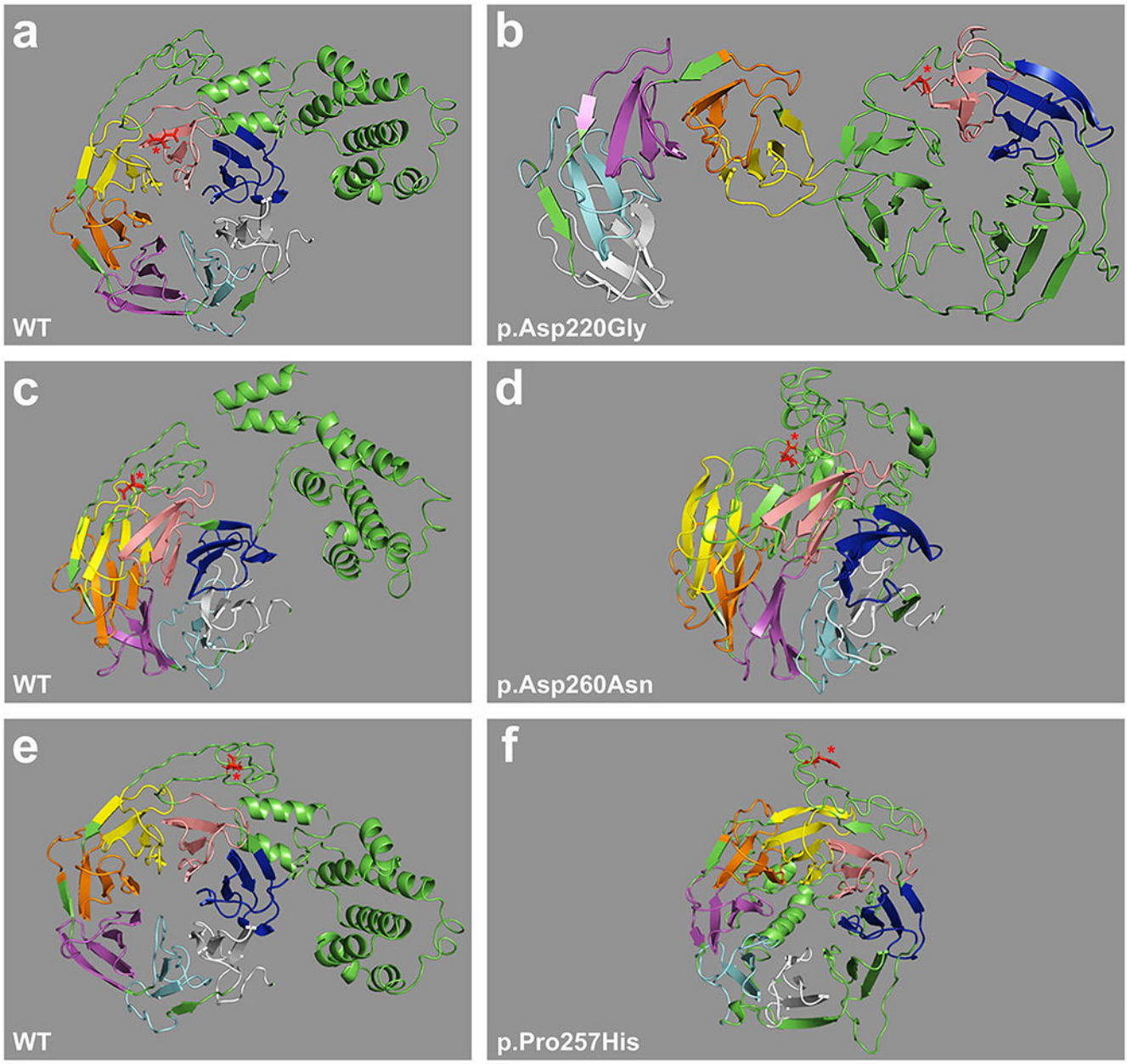

Fig. 2.

In silico modeling of wild-type and C-terminal mutant proteins. Predicted 3D structures for wild-type (NP_054742.2) (**a**, **c**, **e**) and mutant p.(Asp220Gly) (**b**), p.(Asp260Asn) (**d**), and p.(Pro257His) (**f**) full-length polypeptides, modeled using I-Tasser. The location of the mutated amino acid is indicated with red color and asterisk in each pairing

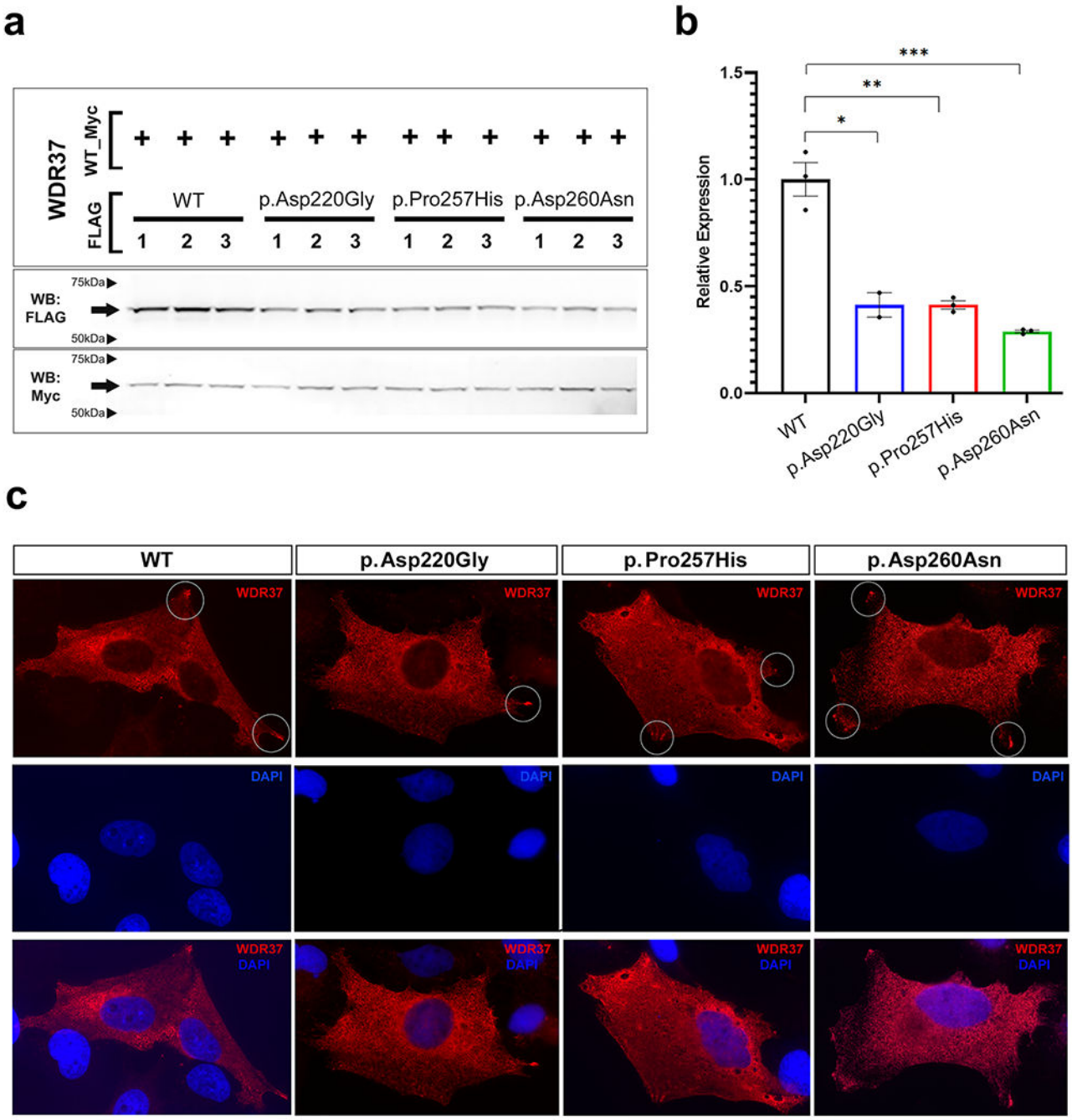

Fig. 3.

Expression and localization of WDR37 wild-type and novel mutant proteins. **a** Western blot (WB) analysis from co-transfection experiments showing expression of wild-type and mutant WDR37 proteins. The positions of bands corresponding to FLAG- or Myc-tagged WDR37 proteins are shown with black arrows. The positions of protein molecular weight size markers are indicated with arrow-heads. **b** Quantification of Western blot results showing statistically significant reduction in the expression of the three novel mutants. $*p < 0.05$, $**p < 0.01$, $***p < 0.001$. **c** Immunocytochemistry data showing localization of

wild-type and mutant proteins after transfection into human B3 lens epithelial cells. White circles indicate enrichment at the leading edge of the spreading cells

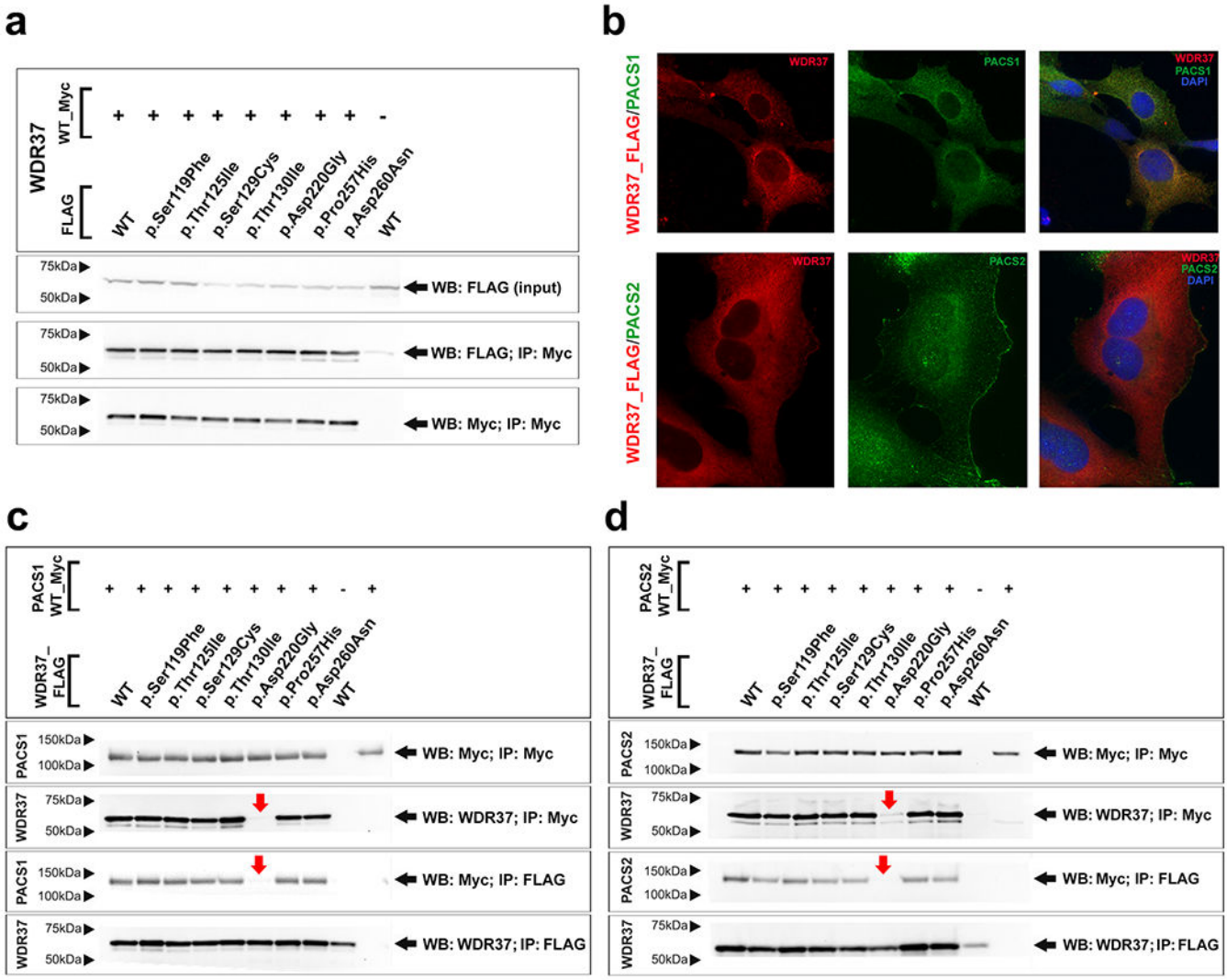

Fig. 4.

Binding capabilities of wild-type and mutant WDR37. **a** Wild-type and mutant WDR37 (both previously reported and novel) are able to form dimers. The positions of FLAG- or Myc-tagged WDR37 proteins are shown with black arrows. **b** Immunocytochemistry showing colocalization of FLAG-tagged WDR37 and PACS1 or PACS2 in transfected human lens epithelial cells. **c** Co-immunoprecipitation experiments confirming interactions between WDR37 proteins and PACS1; the positions of the FLAG-tagged WDR37 or Myc-tagged PACS1 proteins are shown with black arrows in the corresponding panels; please note lack of binding between PACS1 and the WDR37_Asp220Gly mutant (red arrow). **d** Co-immunoprecipitation experiments confirming interactions between WDR37 proteins and PACS2; the positions of the FLAG-tagged WDR37 or Myc-tagged PACS2 proteins are shown with black arrows in corresponding panels; again, please note lack of binding between PACS1 and WDR37_Asp220Gly mutant (red arrow). The positions of protein molecular weight size markers are indicated on the left with arrowheads in **a**, **c** and

d. Primary antibody used for Western Blot (WB) or immunoprecipitation (IP) for each experiment is indicated on the right in **a**, **c** and **d**

Table 1

Genetic and phenotypic data for new and previously reported *WDR37* variants

Source	**This study**			**Previously Published cases**									
Case number	**Individual 1**	**Individual 2**	**Individual 3**	**Hay 1**	**Hay 2**	**Hay 3**	**Reis 1**	**Reis 2**	**Reis 3**[d]	**Kanca 2**[d]	**Kanca 3**	**Kanca 4**	**Kanca 5**
Inheritance	De novo	De novo	Inherited[c]	De novo	De novo	De novo	De novo	De novo	De novo	De novo	De novo	De novo	De novo
Nucleotide[a]	c.659A>G	c.778G>A	c.770C>A	c.356C>A	c.344C > T	c.344C > T	c.356C > T	c.389C > T	c.374C > T	c.386C > G	c.356C > T	c.386C > G	c.389C > T
Protein	p.(Asp220Gly)	p.(Asp260Asn)	p.(Pro257His)	p.(Ser119Tyr)	p.(Thr115Ile)	p.(Thr115Ile)	p.(Ser119Phe)	p.(Thr130Ile)	p.(Thr125Ile)	p.(Ser129Cys)	p.(Ser119Phe)	p.(Ser129Cys)	p.(Thr130Ile)
Domain	WD2	Between WD2 & WD3	Between WD2 & WD3	Upstream of WD1	Upstream of WD1	Upstream of WD1	Upstream of WD1	Upstream of WD1	Upstream of WD1	Upstream of WD1	Upstream of WD1	Upstream of WD1	Upstream of WD1
In silico predictions[b]	Dam. by 5/5	Dam. by 2/5 (MT, F)	Dam. by 2/5 (MT, F)	Dam. by 5/5	Dam. by 3/5 (MA, MT, F)	Dam by 3/5 (MA, MT, F)	Dam. by 5/5	Dam. by 4/5 (S, F, MA, MT)	Dam. by 5/5	Dam. by 5/5	Dam. by 5/5	Dam. by 5/5	Dam. by 4/5 (S, F, MA, MT)
CADD score[b]	32	21.8	20.5	27.6	23.2	23.2	28.7	24.3	28	28.4	28.7	28.4	24.3
REVEL score[b]	0.946	0.193	0.119	0.489	0.263	0.263	0.479	0.415	0.43	0.503	0.479	0.503	0.415
gnomAD	NP	NP	NP	NP	NP	NP	NP	NP	NP	NP	NP	NP	NP
Gender	Male	Female	Female	Female	Male	Male	Male	Female	Male	Female	Female	Female	Male
Age	4y	15y	7y	3y	14y	15y	30y	22 m	8y	6y	9 m	19y	6y
Ocular features	ONH, poor vision	Bluish sclera, ptosis, hyperopia	L CAT, L lens-iris adhesions	COL, RET myopia	COL myopia	COL	PA, COL, MI, GL, CAT	PA, MI, COL, RET, ONH	L PA, MI, COL, ONH	COL, L MI, myopia	COL	COL, CAT	CO, MI, GL, ONH aphakia
Hearing loss	−	+	+	−	−	−	−	possible	+	+	−	−	U
DD/CI	Severe (NV, NA)	Severe (NV, NA)	Severe (NV, LA)	Mild	Moderate	Moderate	Severe (NV, LA)	Severe (NV, NA)	Severe (NV, NA)	Severe (NV, NA)	Delayed	Severe (NV, NA)	Severe (NV, NA)
Seizures	−	+	+	+	1 febrile	+	+	+	+	+	+	+	+
Brain anomalies	MYA	DW, CBA, CCA	PV	CCA, CBA	U	U	DW, PV, MYA	DW, PV, CCA, GRY, MYA	DW, CCA, PV, GYR, MYA	CCA, CBA, GYR	CCA, CBA	CCA, CBA, GRY	CCA, CBA, GYR
Microcephaly	+	−	−	−	−	−	+	+	+	+	−	+	U
Dysmorphic features	+ +	+ +	mild	mild	+ +	+ +	+ +	+ +	+ +	+ +	+ +	+ +	+ +
Short stature	− 2.11 SD	7th %ile	−	−	−	−	+	+	−	+	−	+	−

Source	This study			Previously Published cases									
Case number	**Individual 1**	**Individual 2**	**Individual 3**	**Hay 1**	**Hay 2**	**Hay 3**	**Reis 1**	**Reis 2**	**Reis 3[d]**	**Kanca 2[d]**	**Kanca 3**	**Kanca 4**	**Kanca 5**
Tapered fingers	−	+	+	−	−	−	−	+	−	+	−	−	+
Abnl palmar crease	−	+	−	−	−	−	−	+	−	+	+	+	+
Hypermobility/ dislocations	−	−	+	−	+	+	+	−	+	+	−	−	−
Spine anomalies	−	+	+		+	+	+	+	+	−	−	+	−
CHD	−	+	+	−	+	−	+	+	+	+	+	−	+
GU	−	+	+	+	+	+	+	+	+	−	−	+	+
Feeding disorder	+	+	+	−	+	U	+	+	+	+	+	+	−
Other GI	−	−	+	−	−	U	−	−	+	−	−	+	−
Neonatal complications	+	−	+	−	−	−	+	+	+	−	+	+	+
Other findings	Perinatal asphyxia	Possible delayed puberty	Neonatal meningitis (MRSA)	−	Hernia	Hernia	Incompl. puberty, hernia	Early lethality				Delayed puberty	

[a] NM_014023.4

[b] From NSFP accessed through VEP: SIFT (S), PolyPhen2 (PP2), MutationAssessor (MA), MutationTaster (MT), FATHMM-MKL (F); CADD Phred hg19; REVEL

[c] From unaffected mother

[d] Reis 3 is the same patient presented as Kanca 1; Reis 4 is Kanca 2; 5 patients in Aldinger 2019 are duplicates of Kanca 1–5

+ present, − absent, *Abnl* abnormal, *CHD* congenital heart defect; *GU* genitourinary, *GI* gastrointestinal, *NP* allele not present, *U* unknown, *CAT* cataract, *COL* coloboma, *GL* glaucoma, *Incompl* incomplete, *L* left, *MI* microcornea and/or microphthalmia, *ONH* optic nerve hypoplasia, *PA* Peters anomaly/corneal opacity, *RET* retinal anomaly, *CI* cognitive impairment, *DD* developmental Delay, *NV* non-verbal, *NA* non-ambulatory, *LA* limited ambulation, *DW* Dandy–Walker anomaly/variant, *CBA* cerebellar anomaly, *CCA* corpus callosum anomaly, *PV* prominent/enlarged ventricles, *GRY* gyration anomaly, *MYA* myelination anomaly

Hum Genet. Author manuscript; available in PMC 2022 December 01.